processes

MDPI

Article

A Computational Fluid Dynamics Simulation Study on the Variation of Temperature and Pressure in the Container During the Dry Storage Process of Radioactive Metal Oxides

Junxiang Chen [1,2,3], Guanchen Zhou [1,2,4], Dehui Wu [1,2,*], Peng Zhang [1,2], Fei Xie [1,2,5], Jiapeng Liu [1,2] and Weimin Yang [3]

[1] Beijing Nuclear Chemical Research & Design Institute, China Nuclear Power Engineering Co., Ltd., Beijing 100840, China; chenjxc@cnpe.cc (J.C.); zhougca@cnpe.cc (G.Z.); zhangpenge@cnpe.cc (P.Z.); xiefei@cnpe.cc (F.X.); liujpb@cnpe.cc (J.L.)
[2] Nuclear Fuel Reprocessing Engineering Technology Research Center, China National Nuclear Corporation, Beijing 100840, China
[3] College of Mechanical and Electrical Engineering, Beijing University of Chemical Technology, Beijing 100029, China; yangwm@mail.buct.edu.cn
[4] State Key Laboratory of Precision Welding & Joining of Materials and Structures, Harbin Institute of Technology, Harbin 150001, China
[5] School of Mechanical Engineering & Automation, Beihang University, Beijing 100191, China
* Correspondence: wudh@cnpe.cc

Abstract: Radioactive metal oxides are highly radioactive, hygroscopic spent fuel reprocessing products generally stored in container-sealed dry storage. During the storage process of metal oxides, a large amount of heat is generated due to radioactive decay, and helium is produced by α-decay, which leads to an increase in the temperature and pressure of the storage container. In order to ensure the safety of the radioactive metal oxides in the long-term storage process, computational fluid dynamics simulations are used to investigate the effects of storage conditions on the temperature and pressure of the container. Based on a large amount of simulated temperature data under different storage conditions, a power function is used to construct a mathematical model of ventilation speed, ventilation temperature, stack density, loading volume, heating power, water content, and cumulative helium mass versus metal oxide temperature to obtain a safe, reliable, and economical storage method. The results show that reducing the loading volume and increasing the density of metal oxides, increasing the ventilation speed, and lowering the ventilation temperature are beneficial to the heat transfer and cooling in the dry storage process; increasing the density of metal oxides and lowering the water content of metal oxides and increasing the ventilation temperature and speed are beneficial to avoid the high pressure inside the container. Based on the optimized storage conditions, the temperature peak in the storage process occurs near 25 years, and its temperature reaches 527.6 K. The mathematical model of storage temperature constructed in this study has high computational accuracy, and the maximum relative error of storage temperature is less than 1.80%.

Keywords: radioactive metal oxides; dry storage temperature and pressure; computational fluid dynamics; power function mathematical models

check for updates

Academic Editor: Blaž Likozar

Received: 3 March 2025
Revised: 16 April 2025
Accepted: 17 April 2025
Published: 19 April 2025

Citation: Chen, J.; Zhou, G.; Wu, D.; Zhang, P.; Xie, F.; Liu, J.; Yang, W. A Computational Fluid Dynamics Simulation Study on the Variation of Temperature and Pressure in the Container During the Dry Storage Process of Radioactive Metal Oxides. *Processes* **2025**, *13*, 1240. https://doi.org/10.3390/pr13041240

Copyright: © 2025 by the authors. Licensee MDPI, Basel, Switzerland. This article is an open access article distributed under the terms and conditions of the Creative Commons Attribution (CC BY) license (https://creativecommons.org/licenses/by/4.0/).

1. Introduction

Radioactive metal oxides are a kind of reprocessing product of the nuclear industry and have the characteristics of high radioactivity and easy moisture absorption, etc., in which radioactive decay will continue to release a large amount of heat, α-decay generates

helium, and moisture generates hydrogen due to irradiation [1–5]. In this regard, the nuclear industry generally adopts special storage containers to store them in a hermetically sealed manner [6]. The release of heat and the generation of hydrogen and helium during the storage phase of this metal oxide lead to an increase in the temperature and pressure of the container, which poses a more significant challenge for its safe storage.

There have been many reports on simulation studies in the field of nuclear energy concerning the decay heat export process during the storage of spent fuel. Bae studied temperature changes during the dry storage of multiple spent fuel rods under the effect of additives and found that the addition of additives can significantly benefit the cooling down of spent fuel during dry storage [7]. Benavides' computational fluid dynamics approach to studying the influence of the gap between the inner and outer containers on the export of decay heat during dry storage of spent fuel showed that the size of the gap between the inner and outer containers not only affects the temperature distribution but also affects the temperature distribution of decay heat, which is the most important factor in the dry storage of spent fuel [8]. Zuo studied the heat transfer process of the QM400 spent fuel dry storage equipment at Qinshan Nuclear Power Station in the third phase and found that the heat transfer process involves natural convection, heat conduction, and coupled heat transfer and thermal radiation, and the simulation results match well with the experimental data [9]. Tseng numerically investigated the heat transfer performance of a new tubular dry storage system in storing 61 spent fuel rods using computational fluid dynamics [10]. Wang investigated the airflow pattern as well as the heat transfer characteristics during the dry storage of spent fuel using wind tunnel experiments and computational fluid dynamics [11]. The above spent fuel decay heat calculation objects are spent fuel elements unloaded from nuclear power plants, the energy of which is relatively low. After the reprocessing of spent fuel, radioactive metal oxides with high energy density are obtained, which have high energy density and more stringent storage conditions. Since there are only nine countries that have mastered the technology of spent fuel reprocessing, they are France, Russia, the UK, India, Japan, the United States, Belgium, Germany, and China. As a product of spent fuel reprocessing metal oxides, few studies have been reported. At present, except for the DOE-STD-3013-2012 standard [12] of the U.S. Department of Energy, which consists of theoretical calculations and experimental monitoring of the temperature of the dry storage of plutonium dioxide, there is no report on CFD simulation of the change rule of the temperature of the dry storage container of metal oxides. The U.S. Department of Energy (DOE) has used theoretical calculations to roughly evaluate the storage temperature and pressure of metal oxides, and experimental monitoring is only one-sided storage conditions.

In order to realize the safe storage of radioactive metal oxides, this study adopts a numerical model to verify the reasonableness of the container and explore the influence of the storage conditions on the container temperature and pressure based on its storage characteristics. Based on a large number of simulated temperature data under different storage conditions, the power function mathematical model is used to construct a mathematical model of the relationship between the ventilation air velocity, ventilation temperature, stack density, loading volume, heating power, water content, and the cumulative mass of helium and the temperature of the metal oxides. Oxide temperature is used to obtain a safe, reliable, and economical storage method.

2. Calculation Conditions and Methods

2.1. Radioactive Metal Oxide Storage Containers

The storage containers for metal oxides are shown in Figure 1. The metal oxides are loaded into the inner container, and the sealing of the inner container is realized through threading. Five inner containers are loaded into one outer container, and then the sealing of

the outer container is realized through welding. Inner containers are numbered 1 to 5 from top to bottom. The inner and outer containers are made of 304 stainless steel, with an inner container size of Φ 150 mm × 180 mm and an outer container size of Φ 210 mm × 1175 mm. The inner container has a volume of about 2.255 L, the designed filling capacity is 3.0 kg, and the actual filling capacity is between 2.6 and 3.2 kg.

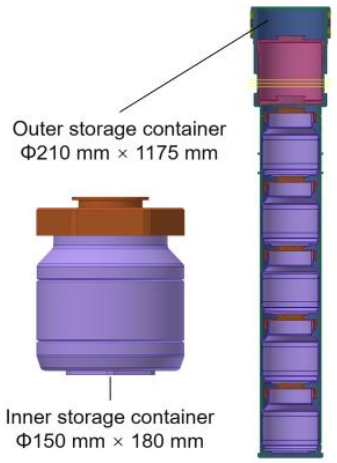


Figure 1. Radioactive metal oxide storage containers.

2.2. Materials and Their Properties

Radioactive metal oxides consist of five isotopes with a density of 11,460 kg/m^3. The average metal content in 1 kg of the metal oxide is about 0.8822 kg. The power of heat release from the metal oxide due to radioactive decay and the cumulative amount of helium produced due to α-decay are shown in Figure 2.

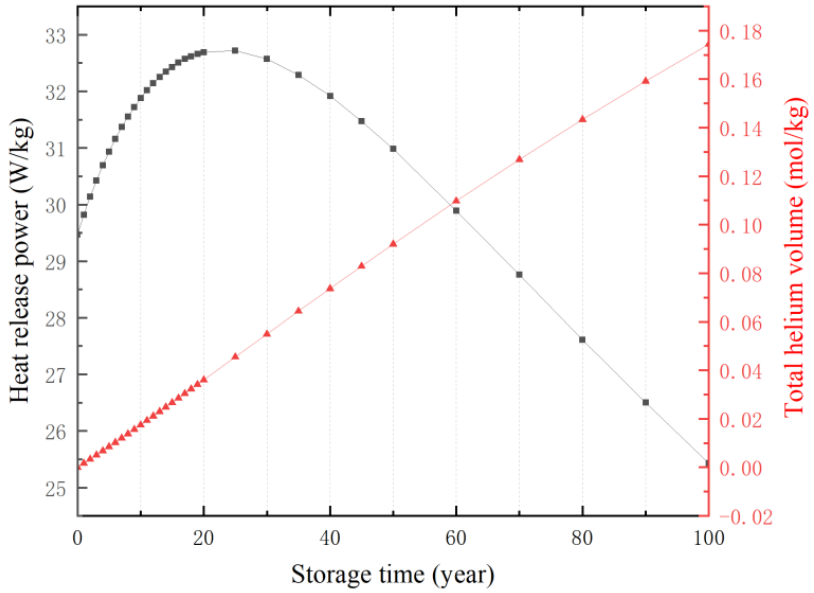


Figure 2. Radioactive metal oxide heat release power and cumulative amount of helium produced.

The density, specific heat, thermal conductivity, viscosity, and radiation coefficient of the material all affect the heat transfer of metal oxides. The densities of air, hydrogen, and helium were calculated at 308 K at atmospheric pressure. Considering that the storage temperature is mainly around 500 K, the specific heat, thermal conductivity, and viscosity of the three gases are calculated at 500 K. The specific heat and thermal conductivity of the metal oxides were calculated based on the formulas reported in the literature [11], as shown in Equations (1) and (2). λ, A_m, N_p, C_p, and T are thermal conductivity (W/m·K),

elemental mass content, mass content, specific heat (J/kg·K), and absolute temperature (K), respectively. According to the literature, the Am content in metal oxides is low, about 0.0006~0.0026 [13–15]. Stainless steel 304 belongs to the nickel-chromium alloy, and its radiation coefficient is taken as a median of 0.45, according to the radiation coefficient range of frosted nickel-chromium alloy, 0.3~0.6. The physical property data used in this study are shown in Table 1.

$$\lambda(W/m{\cdot}K) = (0.3583\ A_m + 0.06317\ N_p + 0.01595 + 0.0002494\ T)^{-1} \quad (1)$$

$$C_p\ (J/kg{\cdot}K) = 68{,}061{,}313.87\ e^{474.5/T}/[T^2(e^{474.5/T}-1)^2 + 0.03408\ T] \quad (2)$$

Table 1. Physical property data.

	Air	Water Vapor	Hydrogen	Helium	304 Stainless Steel	Radioactive Metal Oxides
Density (kg/m^3)	1.146	0.71223	0.080	0.158	7900	11,460
Specific heat (J/kg·K)	1030	2984	14,520	5193	500	297
Thermal conductivity (W/m·K)	0.0407	0.0436	0.266	0.22	18	7
Viscosity (Pa·s)	2.7×10^{-5}	1.67×10^{-5}	1.26×10^{-5}	2.83×10^{-5}	/	/
Emissivity	/	/	/	/	0.45	/

2.3. Simulation of Areas and Meshing

Based on the container storage method, the space area for numerical simulation was defined as 2000 mm × 2000 mm × 2000 mm, and the outer container was placed in the center of this area. In order to facilitate the production of high-quality meshes, the storage containers were regularized while maintaining the effective volume of the inner storage containers, and the air between the inner and outer containers was also regularized. The wall thickness of the inner container was regularized as a 4 mm cylinder, and the five inner containers were placed in the outer bottle in the form of a top and bottom stack. In order to reduce the number of grids and the workload of simulation calculation, according to the principle of symmetry, the simulation area is halved, and the corresponding containers are cut in half vertically from the center of the axis so that the corresponding gridding and simulation calculation area coordinates range from X = −1000 mm~1000 mm, Y = 0 mm~1000 mm, and Z = −1000 mm~1000 mm. The meshes and mesh sensitivity analysis are shown in Figure 3, and the maximum temperature of the metal oxides inside the five inner containers (storage conditions: cooling air temperature 308 K, storage for 25 years) is used as an index for the sensitivity analysis of the number of meshes. The results show that when the number of meshes reaches about 550,000, the temperature change of the metal oxides inside the five inner containers is insensitive. Therefore, the number of hexahedral meshes used in this paper is 556,607, and the maximum mesh skewness is 0.4153.

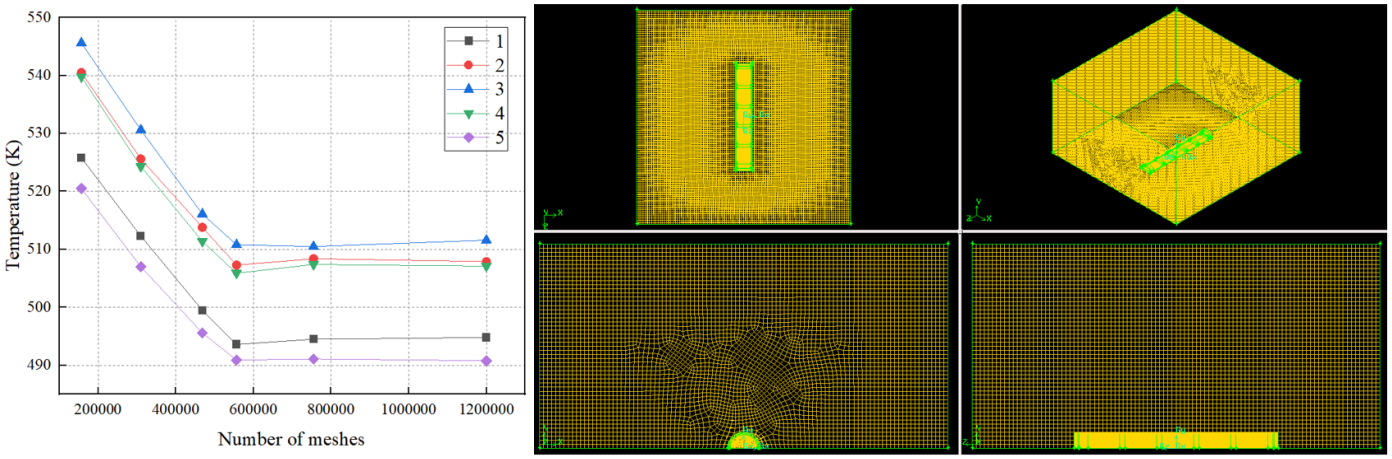


Figure 3. Simulate the meshing of areas and storage containers.

2.4. Calculation Method and Boundary Conditions

Fluent 15.0 software was used for the calculations in this study. The mass transfer model was used, and the DO radiative heat transfer model was turned on by considering component diffusion and heat diffusion. The external environment of the storage vessel is mechanically ventilated, the k-ω turbulence model is used, and the laminar flow model is used for the gas flow in the outer vessel and inner vessel. The heat transfer process in this study involves natural convection, forced convection, heat conduction, and thermal radiation heat transfer (the relevant governing equations are shown in Appendix A). The charging space of the metal oxide is set to the porous media area, the porous medium solid is the metal oxide, and the void is a mixture of air, hydrogen, and helium. The porosity of the porous medium is determined by the mass of the metal oxide charge, the density of the metal oxide, and the effective volume of the inner container. The viscous resistance (symbol $1/\alpha$, unit $1/m^2$) and inertial resistance (symbol C, unit $1/m$) in the porous media region were estimated according to Ergun's empirical formula.

The heat released from the decay of the metal oxides is added to the charging area of the inner packaging through an energy source term (N) in W/m^3. The energy source term is calculated based on the charging mass of the metal oxide (m in kg), the volume of the charging area (V in m^3), and the heating power (P in W/kg) corresponding to the year of storage of the metal oxide in this simulation; its calculation formula is shown in Equation (3), where 0.8822 is the conversion factor of the mass of the metal oxide to the mass of the metal.

$$N = 0.8822\ mP/V \quad (3)$$

The outer container is placed vertically. Horizontal ventilation means that the cooling air is blown from the side of the outer vessel, while vertical ventilation means that the cooling air is ventilated upward from the bottom of the outer vessel. The ventilation inlet is the velocity inlet, while the air outlet is the pressure outlet; the XZ profile of the simulation area is set as the symmetric surface, and the remaining external surface of the air is set as the adiabatic wall. The heat transfer at the air-solid interface is set as the coupled heat transfer mode, and the material of the vessel wall is set as stainless steel, with its corresponding radiation coefficient set as 0.45. The density of the gas mixture in the inner vessel is calculated according to the total mass of air, hydrogen, and helium, along with the volume of the inner vessel. Then, the density data are imported through the UDF. The mass of the three gas mixtures is distributed directly into the inner vessel after initialization based on the mass fraction of each gas.

This simulation requires the determination of both temperature and pressure data. The floating operating pressure setting and the unsteady state simulation method can be used to calculate temperature and pressure data. However, this method requires too much computation and is very time-consuming. For this reason, this simulation first uses the steady-state simulation method to obtain reasonable temperature data. Then, it calculates the pressure based on the amount of gas substance, temperature, space volume, and gas equation of state. The above method can greatly reduce calculation time and, at the same time, can ensure the accuracy of the calculated temperature and pressure data. Based on a large number of temperature data obtained under different storage conditions, a power function empirical mathematical model was used to construct mathematical relationships between the gas velocity, cooling air temperature, stack density, loading volume, heating power, water content, and cumulative mass of helium and various temperatures, and to obtain the model parameters in order to provide mathematical tools for the calculation of temperatures and pressures after changes in metal oxides and storage conditions in engineering applications.

The influencing factors examined in this study include the cooling air ventilation method, the cooling gas ventilation rate, the cooling gas temperature, the inner container filling mass, the heat release power of the metal oxides, the metal oxide water content, the helium cumulant mass, and the stack density of the metal oxide filling. Due to the limitation of the single factor, the maximum temperatures of metal oxides were calculated for 188 sets of different storage conditions, and a power function form was used to construct mathematical models for temperature and seven factors.

For the accounting of gas pressure, the ideal gas equation of state, the van der Waals equation, and the RK equation can calculate the pressure change data of mixed gases, and the errors between them are small so that the calculation of the pressure of mixed gases can meet the requirements of calculation accuracy. In order to facilitate the calculation, the ideal gas equation of state is used in this study for gas mixture pressure accounting.

3. Results and Discussion

3.1. Effect of Ventilation Process Parameters on the Temperature of Radioactive Metal Oxides

Figure 4 shows the effect of the ventilation method and air velocity on the maximum temperature of metal oxides at a ventilation temperature of 308 K for an inner container filled with 3 kg of metal oxides with a moisture content of 0.5% and a stack density of 2200 kg/m^3 for 25 years of storage. The temperature decreases with increasing cooling air velocity for horizontal and vertical ventilation. It indicates that increasing the cooling air intake velocity favors the cooling of metal oxides. At high cooling air velocities (0.7 m/s and 0.9 m/s), the cooling effect of vertical ventilation on metal oxides is better than that of horizontal ventilation; when the air velocity is equal to or less than 0.5 m/s, the difference between the cooling effect of horizontal and vertical ventilation is not apparent.

In order to clarify the temperature distribution inside the storage vessel, Figure 5 shows the temperature cloud for a lateral wind speed of 0.5 m/s. The top and bottom inner containers are cooled by heat transfer more quickly than the middle three containers, resulting in significantly lower temperatures in the top and bottom inner containers than in the middle three inner containers, where the temperature of the middlemost container is the highest, at about 512 K. The temperatures in the area where the metal oxide particles are in contact with the wall surface of the charging bottle are lower than those in the center area since the heat transfer effect makes it easier for heat to be transferred out of the vicinity of the wall surface. The heat in the center region is more challenging to transfer.

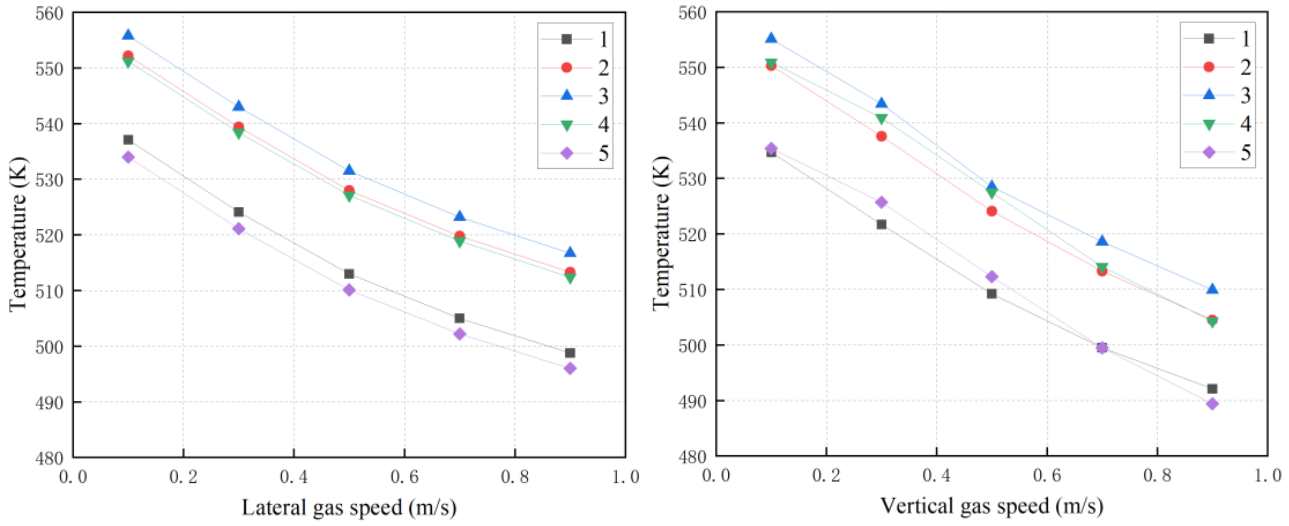


Figure 4. (**a**) The effect of lateral gas speed on the temperature of the inner container; (**b**) The effect of vertical gas speed on the temperature of the inner container.

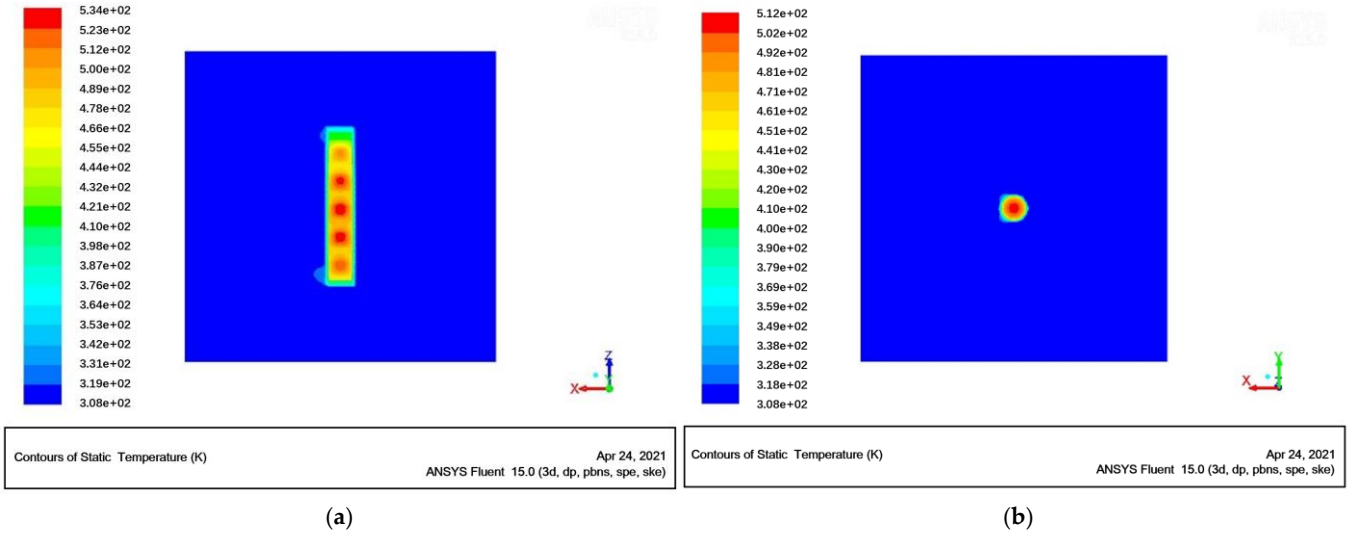


Figure 5. Temperature distribution of transverse wind speed of 0.5 m/s for 25 years: (**a**) Temperature distribution on Y = 0 profile; (**b**) Temperature distribution on Z = 0 profile.

The effect of ventilation gas temperature on the temperature of the storage vessel is shown in Figure 6, which demonstrates the maximum temperature of metal oxides stored for 25 years in each of the five inner containers at ventilation temperatures from 298 K to 323 K, respectively. The maximum temperatures of metal oxides keep increasing linearly with the increase in ventilation gas temperature. When the ventilation temperature is lower than 308 K, due to the low ventilation temperature, the outermost container dissipates heat quickly, and the heat is conducted from the middlemost container to the two ends, which is manifested as the highest temperature of the middlemost container. When the ventilation temperature is greater than or equal to 313 K, the heat dissipation of the outermost container is not effective, resulting in the middle three containers reaching thermal equilibrium.

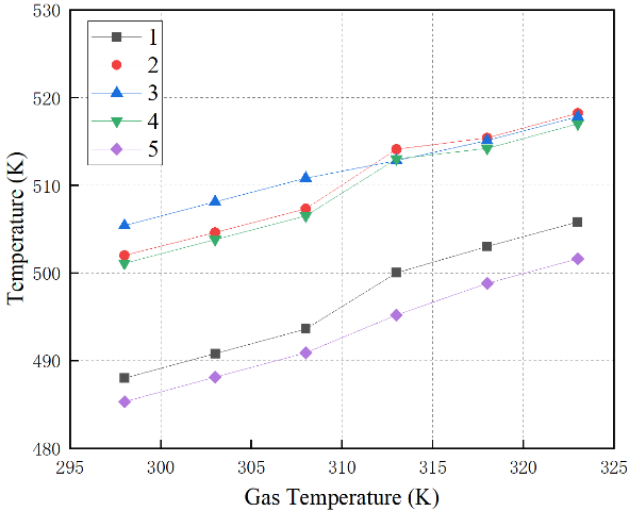


Figure 6. Effect of ventilation gas temperature on the maximum temperature of metal oxides in five inner containers at 25 years.

3.2. Effect of Metal Oxide Filling and Moisture Content on Temperature

Figure 7 shows the maximum temperature of metal oxides with 0.5% water content stored for 25 years at a gas velocity of 0.5 m/s and an air temperature of 308 K. The temperature of the metal oxides is shown in the figure. The more the container is filled with metal oxides, the higher its temperature, with the maximum temperature occurring in the third container. As the mass of the metal oxide is larger, its heat generation is larger. Under the same storage conditions, the transfer of energy becomes more difficult with the increase in the mass of the filling, which ultimately leads to an increase in the temperature of the metal oxide.

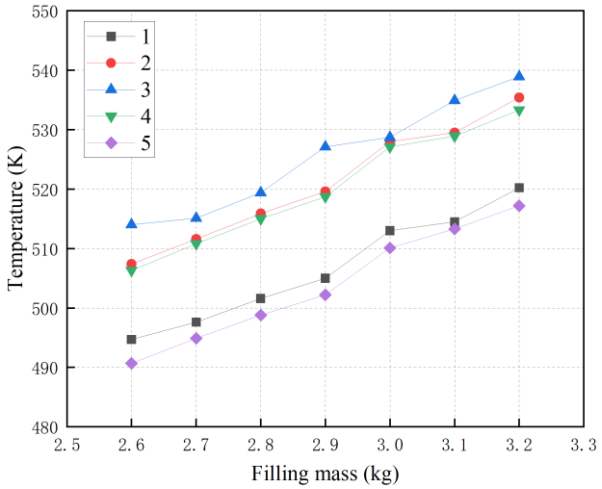
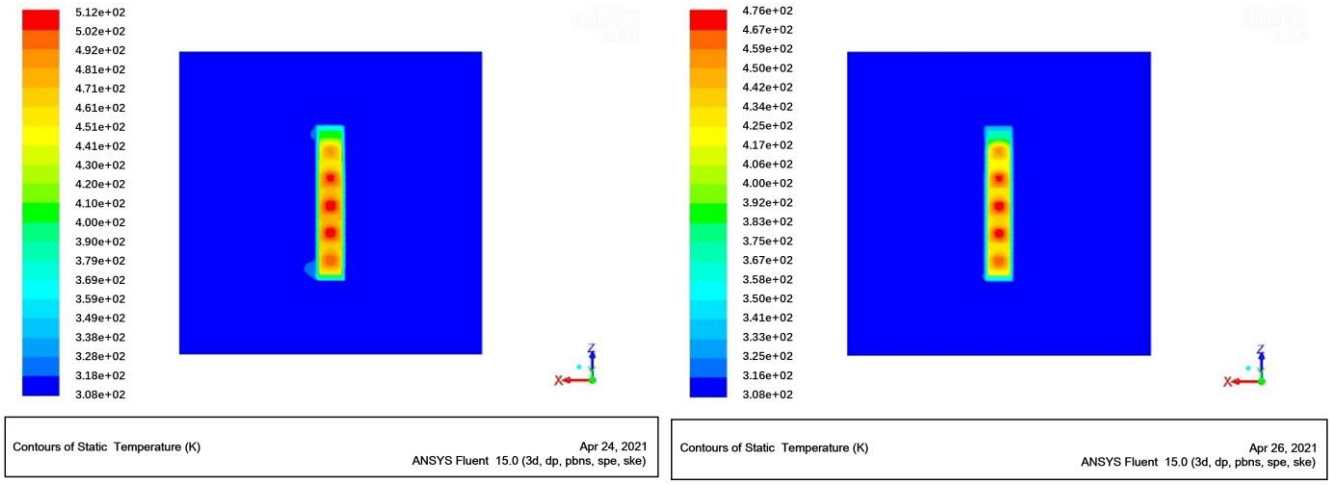


Figure 7. Effect of filling mass on maximum temperature of metal oxides in five inner containers at 25 years.

Water in metal oxides is converted to water vapor at high temperatures, and water vapor is converted to hydrogen in a radiation environment. When the metal oxide is dry, 1 kg of the metal oxide produces about 0.00495 mL to 0.01021 mL of hydrogen per day; when the relative humidity of the water vapor is 50%, 1 kg of the metal oxide produces about 0.00911 mL to 0.18333 mL of hydrogen per day. When 3 kg of the metal oxide has a water content of 0.5%, the mass of the water is 15 g, and the corresponding standard volume of hydrogen gas is about 18,666.7 mL. According to the upper limit of the rate of hydrogen produced by irradiation under dry conditions, it takes about 1669 years to

irradiate water into hydrogen completely; according to the maximum rate of hydrogen produced by irradiation when the relative humidity of water vapor is 50%, it takes about 93 years to irradiate into hydrogen completely. This shows that it takes a long time for water to be converted entirely to hydrogen due to the irradiation of metal oxides. Since it is difficult to characterize the amount of water vapor and hydrogen produced quantitatively, we calculated the temperature distribution in two states, where water vapor is completely converted to hydrogen and is not converted to hydrogen at all. As shown in Figure 8, when 0.5% water in the metal oxide is completely converted to water vapor, the heat transfer effect is better than the conversion to hydrogen. The temperature difference between the two cases can be up to 64.5 K. This is due to the absorption ability of water vapor for infrared wavelengths, which leads to the fact that the water vapor can absorb radiative heat transfer, which is conducive to enhancing the heat transfer effect of the gas mixture on the heat production of the metal oxide.



(**a**) (**b**)

Figure 8. Effect of 25-year storage gas type on the maximum temperature of metal oxides: (**a**) hydrogen; (**b**) water vapor.

Since the irradiation of water into hydrogen is more unfavorable to the storage of metal oxides, according to the conservative principle, we assume that all the water in the metal oxides is irradiated into hydrogen and carry out the calculation of the temperature of the metal oxides with a water content of 0.5~1.5% stored for 25 years, in which the other boundary conditions are as follows: transverse air velocity of 0.5 m/s, air temperature of 308 K, loading of 2.8 kg, and the density of the heap is 1331 kg/m^3. The results of the computational fluid dynamics simulation are shown in Figure 9. The temperature of the metal oxide decreases with the increase of water content. The temperature of the metal oxide with 1.5% water content is 15.7 K lower than that of the metal oxide with 0.5% water content, which is mainly due to the fact that hydrogen generated by water irradiation has a better heat transfer property than that of air and helium.

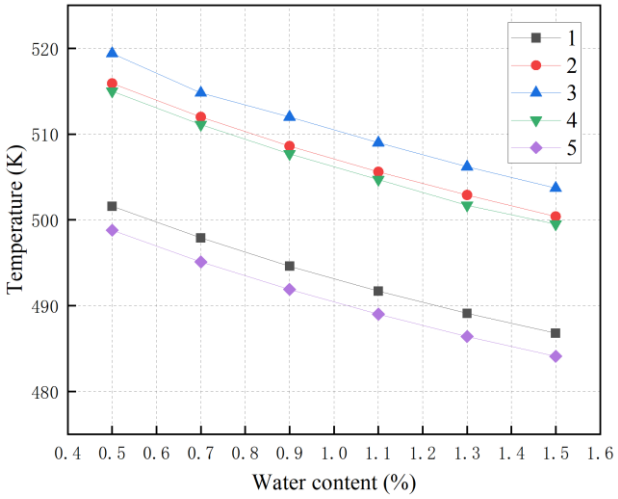


Figure 9. Effect of moisture content on the maximum temperature of metal oxides after 25 years of storage.

3.3. The Effect of Storage Year and Bulk Density on Temperature

Figure 10 shows the temperature variation with time during storage of metal oxides with 0.5% water content at a gas velocity of 0.5 m/s, an air temperature of 308 K, and a pile density of 1331 kg/m^3. Temperature variations in all inner containers showed an increase and then a decrease, with the peak time occurring in the 25th year. The temperature variation with time can be regressed using a 5th-order polynomial, and the model parameters are shown in Table 2. The polynomials are shown in Equation (4), where a_0, a_1, a_2, a_3, a_4, and a_5 are polynomial coefficients and n is the year.

$$T = a_0 + a_1 n + a_2 n^2 + a_3 n^3 + a_4 n^4 + a_5 n^5 \quad (4)$$

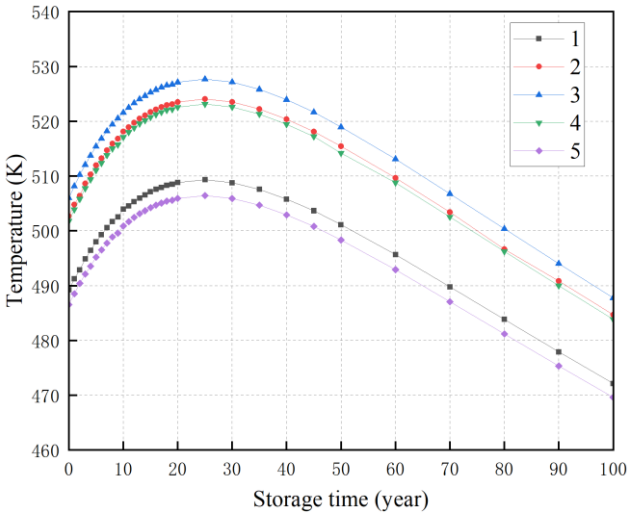


Figure 10. Variation of radioactive metal oxide maximum temperature with storage time.

The tightness of metal oxide stacking in the vessel mainly affects the thermal conductivity and heat transfer. In order to investigate the effect of stacking density on heat transfer, the lower region of each inner container was therefore partitioned and gridded according to different stacking densities (2200 kg/m^3, 2500 kg/m^3) corresponding to the loading height. Under normal storage conditions (air velocity of 0.5 m/s, air temperature of 308 K, and moisture content of 0.5%), simulations were performed to calculate the temperature trends as the storage year changed. Figures 10 and 11 show the variation of metal oxide tempera-

ture with time for heap densities of 1331 kg/m^3, 2200 kg/m^3, and 2500 kg/m^3, respectively. The temperature corresponding to the heap density of 1331 kg/m^3 is obviously higher than that at other heap densities, while the difference between the mutual temperatures of the heap densities of 2200 kg/m^3 and 2500 kg/m^3 is less obvious. The metal oxides showed the highest material temperatures in the third inner container under normal dry storage conditions, with peak temperatures occurring near the 25th year at a maximum of 527.6 K.

Table 2. Five polynomial parameters.

Number	a_0	a_1	a_2	a_3	a_4	a_5
1	489.3	2.038	-6.98×10^{-2}	9.79×10^{-4}	-7.16×10^{-6}	2.14×10^{-8}
2	502.7	2.167	-7.41×10^{-2}	1.05×10^{-3}	-7.74×10^{-6}	2.35×10^{-8}
4	506.1	2.184	-7.45×10^{-2}	1.04×10^{-3}	-7.59×10^{-6}	2.26×10^{-8}
4	501.9	2.145	-7.26×10^{-2}	9.97×10^{-4}	-7.10×10^{-6}	2.06×10^{-8}
5	486.7	2.001	-6.80×10^{-2}	9.43×10^{-4}	-6.80×10^{-6}	2.01×10^{-8}

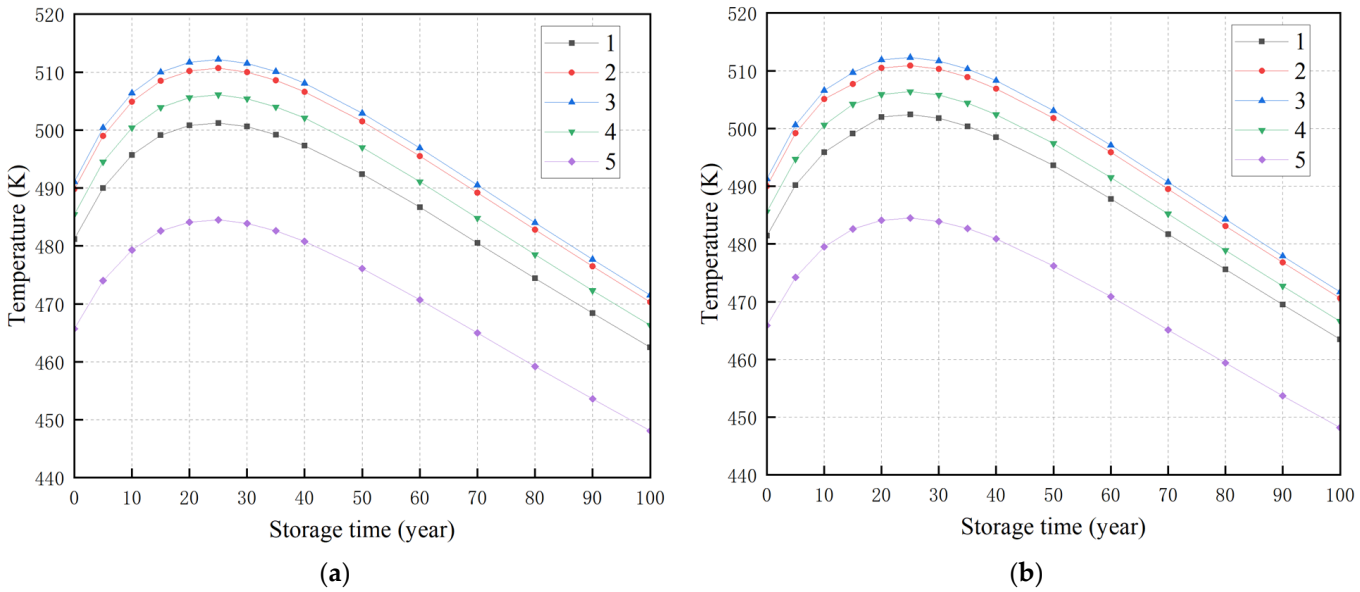


Figure 11. Temperature variation of metal oxides with different bulk densities with year: (**a**) 2200 kg/m^3; (**b**) 2500 kg/m^3.

3.4. Construction of a Mathematical Model of Temperature Power Function

Although the above study can show the trend of the influence of individual factors on the temperature of metal oxides, it is not comprehensive enough, and its application in practice is not convenient enough. For this reason, in this study, based on 188 sets of simulated temperature data (188 sets of data are shown in Appendix B) under lateral ventilation conditions, the power function form is used to construct the mathematical model of temperature and seven factors (air velocity, air temperature, loading volume, moisture content, heating power, stack density, and cumulative helium volume). The power function is shown in Equation (5). T, x_1, x_2, x_3, x_4, x_5, x_6, and x_7 denote the absolute temperature (K), gas velocity (m/s), charge (kg), heating power (W/kg), water content (%), air temperature (K), accumulated helium amount (mol/kg), and the heap density of the metal oxides (g/cm^3), respectively, and b_0~b_7 are the model parameters. Since the power function independent variable cannot be zero, the independent variable for the accumulated helium amount is represented in the form of plus one.

$$T = b_0 {x_1}^{b1} {x_2}^{b2} {x_3}^{b3} {x_4}^{b4} {x_5}^{b5} (1 + x_6)^{b6} {x_7}^{b7} \quad (5)$$

The parameters b_0~b_7 of the power functions for various temperatures can be obtained using the nonlinear optimization technique in Matlab R2020a software. The optimized model parameters for various temperatures are shown in Table 3, and the statistical analysis data for the power function are shown in Table 4. According to the statistical parameters of the model in Table 4, the statistical data of the model parameters corresponding to various temperatures can prove that the power function model is suitable. All of them satisfy the judgment criteria of P2 > 0.9 (more significant than 0.9999) and F > 10 FT (=19.9). The correlation index R^2 of the temperature power function model is more significant than 0.986, the average relative error between the calculated value of the temperature model and the simulated value is less than 0.38%, and the maximum relative error between the calculated value of the power function model and the simulated value is less than 1.80%. The effect of the simulated calculated temperature and power function model calculated temperature is shown in Figure 12a–e. Both the model statistics and the simulated regression effect of the data proved that the temperature power function influence model proposed in this study has good accuracy and can be used for temperature calculation in practical work.

Table 3. Parameters of the temperature exponentiation function model.

Number	b_0	b_1	b_2	b_3	b_4	b_5	b_6	b_7
1	1.40×10^{1}	-3.49×10^{-2}	2.25×10^{-1}	3.07×10^{-1}	-1.67×10^{-2}	4.01×10^{-1}	-1.33×10^{-1}	-3.14×10^{-2}
2	1.70×10^{1}	-3.55×10^{-2}	2.33×10^{-1}	3.15×10^{-1}	-1.73×10^{-2}	3.66×10^{-1}	-1.39×10^{-1}	-5.08×10^{-2}
4	1.95×10^{1}	-3.52×10^{-2}	2.40×10^{-1}	3.18×10^{-1}	-1.64×10^{-2}	3.41×10^{-1}	-1.35×10^{-1}	-6.00×10^{-2}
4	1.61×10^{1}	-3.58×10^{-2}	2.33×10^{-1}	3.15×10^{-1}	-1.75×10^{-2}	3.76×10^{-1}	-1.34×10^{-1}	-6.46×10^{-2}
5	1.59×10^{1}	-3.54×10^{-2}	2.26×10^{-1}	3.04×10^{-1}	-1.69×10^{-2}	3.81×10^{-1}	-1.32×10^{-1}	-8.58×10^{-2}

Table 4. Statistical analysis of power function models.

Number	P2	F	10FT	R^2	Mean Relative Error	Maximum Relative Error
1	0.9999	1,076,718	19.9	0.987	0.32	1.49%
2	0.9999	936,846	19.9	0.987	0.35	1.50%
4	0.9999	902,949	19.9	0.987	0.35	1.80%
4	0.9999	838,227	19.9	0.986	0.36	1.59%
5	0.9999	769,284	19.9	0.986	0.38	1.76%

According to the positive and negative relationship between the values of the model parameters, it can be seen that the increase in ventilation air velocity is conducive to reducing the temperature of metal oxides; the reduction of ventilation temperature is conducive to the cooling of metal oxides; an appropriate increase in the water content is conducive to the heat transfer of metal oxides; the increase in the density of metal oxides is conducive to the heat transfer and cooling; the increase in the cumulative helium substance is conducive to the cooling of metal oxides; the higher the amount of loading is, the more unfavorable is the cooling and heat transfer; the higher the power of heat generation is, the less favorable is the cooling of equipment and materials. The higher the heating power of the metal oxide, the more unfavorable it is for cooling.

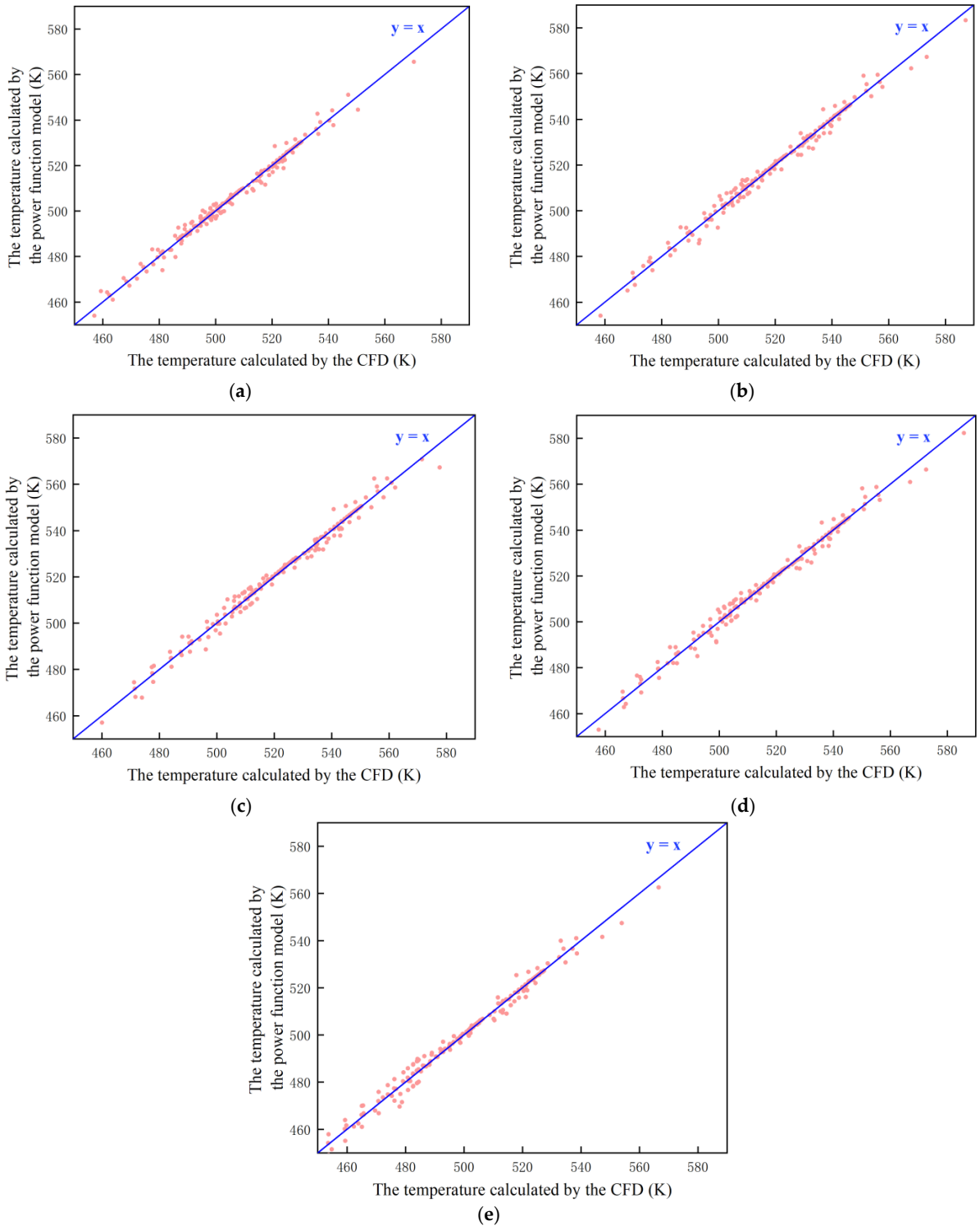


Figure 12. The effect of the power function model of the temperature influencing factors of 1~5 in the inner container: (**a**) inner container 1; (**b**) inner container 2; (**c**) inner container 3; (**d**) inner container 4; (**e**) inner container 5.

3.5. The Pressure of the Storage Vessel Changes Regularly

Figure 13 shows the trend of the gas pressure in the inner vessel with time during storage for metal oxides of different stack densities. The continuous generation of helium from the decay of the metal oxides during storage does not decrease gas pressure even after the temperature peak has passed during storage. At the exact moment, containers with higher temperatures have higher internal pressures. Since the different stack densities of

the metal oxide charge result in different heat transfer of the material, the higher the stack density, the lower the average temperature of the material, so the pressures at the other stack densities (2000 kg/m^3, 2200 kg/m^3, and 2500 kg/m^3) are relatively low compared to the pressure at the 1331 kg/m^3 stack density. The maximum pressure in year 0 is about 17.5 to 18.3 atm, and in 100 years of storage, the maximum pressure is about 24.5 to 25.6 atm.

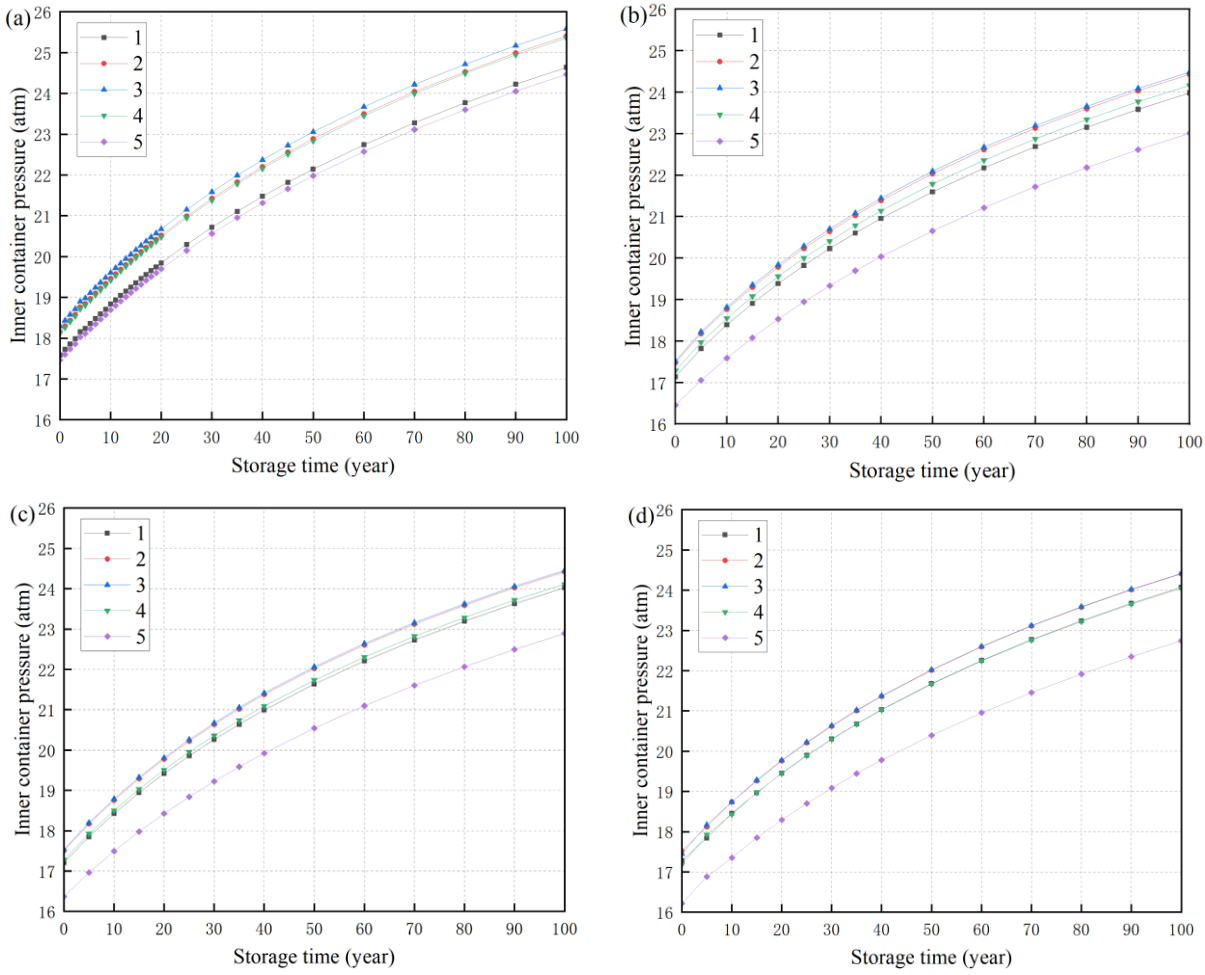


Figure 13. Variation trend of pressure under different filling densities with time: (**a**) 1331 kg/m^3; (**b**) 2000 kg/m^3; (**c**) 2200 kg/m^3; (d) 2500 kg/m^3.

4. Conclusions

In this study, the computational fluid dynamics method was used to study the temperature and pressure changes of radioactive metal oxides during long-term storage, and the influence of storage conditions on the temperature of metal oxides was determined.

The simulation results show that increasing the gas velocity, reducing the air temperature, reducing the amount of material, increasing the bulk density, and having the appropriate amounts of moisture content and cumulative helium content are conducive to the heat transfer and cooling of metal oxides in the dry storage process. The increase of the moisture content of metal oxides is very obvious to the increase of container pressure, and the moisture content needs to be strictly controlled in the actual storage process to avoid excessive container pressure and hazardous events. Based on the optimized storage conditions, the temperature peak during storage occurred around 25 years, and its temperature reached 527.6 K.

The parameter optimization results and statistical analysis of the power function model show that the mathematical model has good reproducibility of the CFD simulation results,

and the maximum relative error of temperature is less than 1.80%. These mathematical models can be used to estimate temperature data during the dry storage of radioactive metal oxides and to calculate the trend of the pressure of the charging vessel based on the temperature, the amount of gaseous mixture, and the volume of the container.

Author Contributions: J.C.: Writing—original draft, formal analysis, and conceptualization; G.Z.: Writing—original draft, methodology, writing—review and editing; D.W.: Visualization, validation, data curation, funding acquisition, project administration and resources; P.Z.: Data curation, writing—review and editing. F.X.: Validation, writing—review and editing; J.L.: Project administration, resources, and supervision; W.Y.: Methodology and resources. All authors have read and agreed to the published version of the manuscript.

Funding: This research received no external funding.

Data Availability Statement: The original contributions presented in this study are included in the article. Further inquiries can be directed to the corresponding author.

Conflicts of Interest: Authors Junxiang Chen, Guanchen Zhou, Dehui Wu, Peng Zhang, Fei Xie and Jiapeng Liu were employed by China Nuclear Power Engineering Co., Ltd. and China National Nuclear Corporation. The remaining author declare that the research was conducted in the absence of any commercial or financial relationships that could be construed as a potential conflict of interest.

Appendix A. Governing Equation

Species Transport Equations:

$$\frac{\partial}{\partial_t}(\rho Y_i) + \nabla\cdot(\rho\vec{v}Y_i) = -\nabla\cdot\vec{J}_i$$

where ρ, t, $\vec{v}$, Y_i, $\vec{J}_i$ denote the fluid density (kg/m^3), time (s), fluid velocity vector, i substance mass fraction and diffusive flux, respectively.

Momentum Conservation Equations:

$$\frac{\partial}{\partial_t}\left(\rho\vec{v}\right) + \nabla\cdot\left(\rho\vec{v}\vec{v}\right) = -\nabla p + \nabla\cdot(\overline{\overline{\tau}}) + \rho\vec{g}$$

where p, $\overline{\overline{\tau}}$ and $\rho\vec{g}$ denote the static pressure (Pa), stress tensor, and gravity (N), respectively

The energy conservation equation:

$$\frac{\partial_T}{\partial_t} + \mu\nabla T = \alpha\nabla^2\mathrm{T} + \mathrm{S}_T$$

where T, μ, α, S_T denote temperature (K), velocity (m/s), heat transfer coefficient (W/m^2·K), and energy source terms, respectively.

DO radiation equation:

$$\frac{d_{I(r,s)}}{d_s} + (a+\delta_s)I(r,s) = an^2\frac{\delta T^4}{\pi} + \frac{\delta_S}{4\pi}\int_0^{4\pi} I(r,s')\Phi(S,S')d\Omega'$$

where I, r, s, a, δ_s, n, δ, Φ, Ω' denote the radiant intensity (W/(m^2·sr)), vector position, vector direction, absorption coefficient, scattering coefficient, refractive index, Stefan Boltzmann constant, phase function and steradian angle.

Appendix B

Table A1. 188 sets of calculation data.

Number	Gas Velocity (m/s)	Loading Capacity (kg)	Heating Power (W/kg)	Water Content (%)	Temperature (K)	He Content (mol/kg)	Metal Bulk Density (g/mL)	Container 1	Container 2	Container 3	Container 4	Container 5
1	0.1	3	28.74	0.5	308	0.03914	1.330565	537.145	552.2699	555.8429	551.2527	534.0904
2	0.3	3	28.74	0.5	308	0.03914	1.330565	524.1371	539.4051	543.0437	538.4351	521.1744
3	0.5	3	28.74	0.5	308	0.03914	1.330565	513.0479	528.0569	531.5979	527.1256	510.1512
4	0.7	3	28.74	0.5	308	0.03914	1.330565	505.0917	519.8278	523.2722	518.9284	502.2502
5	0.9	3	28.74	0.5	308	0.03914	1.330565	498.889	513.3609	516.712	512.4884	496.096
6	0.1	2.6	32.72	0.5	308	0.04549	1.330565	536.143	551.1882	554.8955	550.1825	533.1255
7	0.3	2.6	32.72	0.5	308	0.04549	1.330565	524.2207	539.429	543.2068	538.4631	521.2767
8	0.5	2.6	32.72	0.5	308	0.04549	1.330565	513.3267	528.2923	531.9812	527.3647	510.4476
9	0.7	2.6	32.72	0.5	308	0.04549	1.330565	505.4829	520.1942	523.7903	519.2977	502.6577
10	0.9	2.6	32.72	0.5	308	0.04549	1.330565	499.3544	513.8142	517.3214	512.9443	496.5767
11	0.5	2.8	28.74	0.5	308	0.03914	1.330565	501.6521	515.9109	519.4291	515.0027	498.8542
12	0.5	2.8	28.74	0.7	308	0.03914	1.330565	497.9214	512.0361	514.8926	511.1395	495.1443
13	0.5	2.8	28.74	0.9	308	0.03914	1.330565	494.6691	508.652	512.0793	507.7658	491.9124
14	0.5	2.8	28.74	1.1	308	0.03914	1.330565	491.78	505.6388	509.0253	504.7629	489.043
15	0.5	2.8	28.74	1.3	308	0.03914	1.330565	489.1809	502.922	506.2673	501.7179	486.4652
16	0.5	2.8	28.74	1.5	308	0.03914	1.330565	486.8212	500.4526	503.7636	499.5953	484.1195
17	0.5	3.2	32.72	0.4	308	0.04549	1.330565	540.3311	556.8816	560.9103	555.8722	537.1554
18	0.5	3.2	32.72	0.6	308	0.04549	1.330565	535.7493	552.1458	556.1247	551.1467	532.5905
19	0.5	3.2	32.72	0.8	308	0.04549	1.330565	531.7873	548.0399	551.9722	547.0512	528.6466
20	0.5	3.2	32.72	1	308	0.04549	1.330565	528.2886	544.406	548.2939	543.4272	525.1654
21	0.5	3.2	32.72	1.2	308	0.04549	1.330565	525.1534	541.1427	544.988	540.1731	522.0462
22	0.5	3.2	32.72	1.4	308	0.04549	1.330565	521.027	536.9429	540.7602	535.9863	517.9504
23	0.5	2.6	28.74	0.5	308	0.03914	1.330565	494.7598	507.4124	514.0809	506.3173	490.7511
24	0.5	2.7	28.74	0.5	308	0.03914	1.330565	497.6935	511.6992	515.1636	510.8051	494.946
25	0.5	2.8	28.74	0.5	308	0.03914	1.330565	501.6516	515.9103	519.4284	515.0022	498.8538
26	0.5	2.9	28.74	0.5	308	0.03914	1.330565	505.0896	519.6459	527.1507	518.7581	502.2546
27	0.5	3	28.74	0.5	308	0.03914	1.330565	513.0899	528.0869	528.7826	527.1566	510.1992
28	0.5	3.1	28.74	0.5	308	0.03914	1.330565	514.5036	529.5786	534.9477	528.9687	513.3507
29	0.5	3.2	28.74	0.5	308	0.03914	1.330565	520.2954	535.4878	538.9511	533.3102	517.2822
30	0.5	2.6	32.72	0.5	308	0.04549	1.330565	515.7111	525.4544	534.3521	524.0296	512.5536

Table A1. *Cont.*

Number	Gas Velocity (m/s)	Loading Capacity (kg)	Heating Power (W/kg)	Water Content (%)	Temperature (K)	He Content (mol/kg)	Metal Bulk Density (g/mL)	Container 1	Container 2	Container 3	Container 4	Container 5
31	0.5	2.7	32.72	0.5	308	0.04549	1.330565	516.2839	531.4307	534.9428	530.5165	513.3847
32	0.5	2.8	32.72	0.5	308	0.04549	1.330565	523.746	539.8243	542.5306	538.7047	520.4277
33	0.5	2.9	32.72	0.5	308	0.04549	1.330565	525.3223	540.9587	549.5107	539.9356	522.2878
34	0.5	3	32.72	0.5	308	0.04549	1.330565	529.5656	545.4073	553.8803	544.3884	526.4894
35	0.5	3.1	32.72	0.5	308	0.04549	1.330565	536.4696	553.9206	558.1326	550.75	534.7642
36	0.5	3.2	32.72	0.5	308	0.04549	1.330565	541.802	557.8561	562.1699	556.3515	538.6311
37	0.5	3	24.76	0.5	308	0	1.330565	489.2412	502.6664	505.9976	501.7804	486.5467
38	0.5	3	25.12	0.5	308	0.001388	1.330565	491.2409	504.7942	508.1549	503.9029	488.5263
39	0.5	3	25.47	0.5	308	0.0028	1.330565	492.8645	506.3954	510.2242	505.7972	490.4331
40	0.5	3	25.78	0.5	308	0.004234	1.330565	494.8596	508.6447	512.0582	507.7439	492.1088
41	0.5	3	26.08	0.5	308	0.00659	1.330565	496.4139	510.3013	513.7369	509.38	493.5461
42	0.5	3	26.36	0.5	308	0.007165	1.330565	497.9795	511.9643	515.4228	511.0556	495.1979
43	0.5	3	26.61	0.5	308	0.008659	1.330565	499.3018	513.251	516.8459	512.3689	496.5072
44	0.5	3	26.85	0.5	308	0.01017	1.330565	500.5632	514.714	518.2095	513.7988	497.7562
45	0.5	3	27.07	0.5	308	0.0117	1.330565	501.695	515.9198	519.4317	515.0017	498.8769
46	0.5	3	27.27	0.5	308	0.01324	1.330565	502.5147	516.8244	520.5347	515.7126	499.6035
47	0.5	3	27.45	0.5	308	0.01479	1.330565	503.935	518.125	521.5771	517.1004	500.8893
48	0.5	3	27.62	0.5	308	0.01636	1.330565	504.518	518.9261	522.4785	518.0012	501.6722
49	0.5	3	27.78	0.5	308	0.01794	1.330565	505.2871	519.7441	523.3067	518.8177	502.4343
50	0.5	3	27.92	0.5	308	0.01953	1.330565	505.9747	520.4773	524.0498	519.5492	503.115
51	0.5	3	28.04	0.5	308	0.02113	1.330565	506.5397	521.0797	524.6602	520.1504	503.6745
52	0.5	3	28.16	0.5	308	0.02273	1.330565	507.1002	521.6771	525.2652	520.7465	504.2294
53	0.5	3	28.26	0.5	308	0.02435	1.330565	507.5546	522.1624	525.757	521.2309	504.6796
54	0.5	3	28.35	0.5	308	0.02597	1.330565	507.9534	522.5887	526.189	521.6564	505.0745
55	0.5	3	28.43	0.5	308	0.0276	1.330565	508.2966	522.9559	526.5609	522.0228	505.4142
56	0.5	3	28.5	0.5	308	0.02924	1.330565	508.4558	523.1213	526.7263	522.1887	505.5734
57	0.5	3	28.56	0.5	308	0.03088	1.330565	508.8024	523.5001	527.1125	522.5659	505.9146
58	0.5	3	28.74	0.5	308	0.03914	1.330565	509.3224	524.0659	527.6867	523.1311	506.4285
59	0.5	3	28.73	0.5	308	0.04746	1.330565	508.7933	523.5195	527.1344	522.5865	505.9028
60	0.5	3	28.59	0.5	308	0.05577	1.330565	507.5639	522.2288	525.8279	521.2992	504.6826
61	0.5	3	28.35	0.5	308	0.06405	1.330565	505.7951	520.3644	523.9397	519.4398	502.9293
62	0.5	3	28.04	0.5	308	0.07225	1.330565	503.6618	518.1126	521.6591	517.1938	500.8147

Table A1. *Cont.*

Number	Gas Velocity (m/s)	Loading Capacity (kg)	Heating Power (W/kg)	Water Content (%)	Temper-ature (K)	He Content (mol/kg)	Metal Bulk Density (g/mL)	Container 1	Container 2	Container 3	Container 4	Container 5
63	0.5	3	27.66	0.5	308	0.08037	1.330565	501.142	515.4477	518.9568	514.1892	498.3212
64	0.5	3	26.82	0.5	308	0.09627	1.330565	495.6855	509.674	513.1093	508.7773	492.9119
65	0.5	3	25.9	0.5	308	0.1117	1.330565	489.7879	503.4244	506.7752	502.5445	487.0711
66	0.5	3	24.97	0.5	308	0.1265	1.330565	483.8468	496.6405	500.3779	496.2528	481.181
67	0.5	3	24.05	0.5	308	0.1409	1.330565	477.9371	490.847	494.0234	490.0028	475.34
68	0.5	3	23.15	0.5	308	0.1547	1.330565	472.149	484.6961	487.7855	483.8701	469.6131
69	0.5	3	29.47	0.5	308	0	1.330565	515.648	530.6976	534.4027	529.7456	512.7045
70	0.5	3	29.82	0.5	308	0.001662	1.330565	517.4361	532.5969	536.3265	531.6408	514.4759
71	0.5	3	30.14	0.5	308	0.003347	1.330565	519.0548	534.3156	538.0674	533.3561	516.0804
72	0.5	3	30.42	0.5	308	0.005053	1.330565	520.4489	535.7965	539.5673	534.834	517.4619
73	0.5	3	30.69	0.5	308	0.006778	1.330565	521.795	537.2268	541.016	536.2614	518.7961
74	0.5	3	30.93	0.5	308	0.00852	1.330565	522.9503	538.4541	542.2589	537.4863	519.9409
75	0.5	3	31.16	0.5	308	0.01028	1.330565	524.0623	539.6359	543.4558	538.6657	521.0429
76	0.5	3	31.37	0.5	308	0.01205	1.330565	525.0624	540.699	544.5324	539.7268	522.034
77	0.5	3	31.55	0.5	308	0.01384	1.330565	525.9009	541.591	545.4357	540.6171	522.8651
78	0.5	3	31.72	0.5	308	0.01564	1.330565	526.6836	542.4237	546.279	541.4482	523.6407
79	0.5	3	31.88	0.5	308	0.01746	1.330565	527.4105	543.1973	547.0624	542.2204	524.3612
80	0.5	3	32.02	0.5	308	0.01928	1.330565	528.0317	543.8589	547.7324	542.8808	524.9768
81	0.5	3	32.14	0.5	308	0.02112	1.330565	528.5457	544.407	548.2874	543.4279	525.486
82	0.5	3	32.25	0.5	308	0.02296	1.330565	529.0065	544.8986	548.7853	543.9187	525.9426
83	0.5	3	32.35	0.5	308	0.02481	1.330565	529.4146	545.3346	549.2268	544.3539	526.3469
84	0.5	3	32.43	0.5	308	0.02667	1.330565	529.8269	545.771	549.6687	544.7895	526.7556
85	0.5	3	32.51	0.5	308	0.02853	1.330565	530.0198	545.9828	549.8835	545.001	526.9462
86	0.5	3	32.57	0.5	308	0.0304	1.330565	530.2174	546.1957	550.0995	545.2137	527.1418
87	0.5	3	32.62	0.5	308	0.03228	1.330565	530.3629	546.3535	550.2596	545.3712	527.2856
88	0.5	3	32.66	0.5	308	0.03416	1.330565	530.4567	546.4566	550.3644	545.4743	527.3783
89	0.5	3	32.69	0.5	308	0.03604	1.330565	530.499	546.5052	550.4139	545.5228	527.4199
90	0.5	3	32.72	0.5	308	0.04549	1.330565	530.0911	546.0914	549.9966	545.1104	527.0134
91	0.5	3	32.57	0.5	308	0.05494	1.330565	528.7625	544.7008	548.59	543.7232	525.6936
92	0.5	3	32.29	0.5	308	0.06436	1.330565	526.7705	542.6067	546.4709	541.634	523.7168
93	0.5	3	31.92	0.5	308	0.07369	1.330565	524.3225	540.0284	543.8611	539.0615	521.2882
94	0.5	3	31.47	0.5	308	0.08292	1.330565	521.4639	537.0134	540.8088	536.0534	518.4529

Table A1. *Cont.*

Number	Gas Velocity (m/s)	Loading Capacity (kg)	Heating Power (W/kg)	Water Content (%)	Temper-ature (K)	He Content (mol/kg)	Metal Bulk Density (g/mL)	Container 1	Container 2	Container 3	Container 4	Container 5
95	0.5	3	30.98	0.5	308	0.09202	1.330565	518.4009	533.78	537.5347	532.8274	515.4155
96	0.5	3	29.89	0.5	308	0.1098	1.330565	511.703	526.7011	530.3653	525.7653	508.7756
97	0.5	3	28.76	0.5	308	0.1269	1.330565	504.7922	519.388	522.9567	518.4701	501.9268
98	0.5	3	27.61	0.5	308	0.1434	1.330565	497.7598	511.9378	515.4072	511.0389	494.9602
99	0.5	3	26.5	0.5	308	0.1592	1.330565	490.9318	504.6968	508.0678	503.8171	488.1983
100	0.5	3	25.43	0.5	308	0.1744	1.330565	484.3059	497.6632	500.9369	496.803	481.6388
101	0.1	2.6	20	0.5	298	0.001	1.330565	462.3237	473.5818	477.5601	472.6449	459.7792
102	0.3	2.6	25	0.8	308	0.005848	1.330565	479.4274	499.8259	501.1722	498.9505	476.8293
103	0.5	2.6	30	1.1	318	0.0342	1.330565	500.8981	515.2844	519.2456	514.0279	498.6368
104	0.7	2.6	35	1.5	323	0.02	1.330565	520.7981	529.0453	537.0106	528.1448	511.6222
105	0.5	2.8	20	1.5	308	0.001	1.330565	447.51	458.472	460.0356	457.7251	445.2596
106	0.7	2.8	25	1.1	298	0.005848	1.330565	459.3589	475.5352	478.1026	471.1461	463.9168
107	0.1	2.8	30	0.8	323	0.0342	1.330565	541.3937	556.1682	559.3713	555.1595	538.4053
108	0.3	2.8	35	0.5	318	0.02	1.330565	547.0688	573.4572	571.4847	572.6079	553.9997
109	0.7	3	20	0.8	318	0.02	1.330565	457.0108	467.9837	473.9524	467.2499	454.7843
110	0.5	3	25	0.5	323	0.001	1.330565	495.4417	508.5117	515.1643	507.6671	492.8573
111	0.3	3	30	1.5	298	0.005848	1.330565	517.6426	533.369	537.0793	532.3644	514.5874
112	0.1	3	35	1.1	308	0.0342	1.330565	570.3422	587.1756	591.4796	585.8906	566.6113
113	0.3	3.2	20	1.1	323	0.0342	1.330565	481.1741	493.1647	496.2254	492.3641	478.7879
114	0.1	3.2	25	1.5	318	0.02	1.330565	522.9911	536.7238	542.6828	536.1961	519.9005
115	0.7	3.2	30	0.8	308	0.001	1.330565	514.7444	530.0428	534.2508	529.0965	511.7496
116	0.5	3.2	35	0.5	298	0.005848	1.330565	550.5168	567.9636	577.6766	567.0098	547.3171
117	0.5	3	24.76	0.5	308	0	2	477.5562	486.7126	487.9805	482.7621	465.4873
118	0.5	3	26.36	0.5	308	0.007165	2	489.0691	498.5675	500.08	494.3526	473.9487
119	0.5	3	27.45	0.5	308	0.01479	2	494.7324	504.4777	506.0446	500.2107	479.328
120	0.5	3	28.16	0.5	308	0.02273	2	498.1537	508.0483	509.6519	503.7575	482.6236
121	0.5	3	28.56	0.5	308	0.03088	2	499.7955	509.7627	511.3878	505.4649	484.1731
122	0.5	3	28.74	0.5	308	0.03914	2	500.2001	510.1875	511.8237	505.8955	484.5531
123	0.5	3	28.73	0.5	308	0.04746	2	499.5518	509.5147	511.1532	505.2395	483.9377
124	0.5	3	28.59	0.5	308	0.05577	2	498.1937	508.1015	509.7358	503.8502	482.6515
125	0.5	3	28.35	0.5	308	0.06405	2	496.2943	506.1235	507.7487	501.9018	480.8548
126	0.5	3	27.66	0.5	308	0.08037	2	491.374	500.9958	502.5918	496.8457	476.2069

Table A1. *Cont.*

Number	Gas Velocity (m/s)	Loading Capacity (kg)	Heating Power (W/kg)	Water Content (%)	Temper-ature (K)	He Content (mol/kg)	Metal Bulk Density (g/mL)	Container 1	Container 2	Container 3	Container 4	Container 5
127	0.5	3	26.82	0.5	308	0.09627	2	485.6726	495.049	496.6071	490.9811	470.8306
128	0.5	3	25.9	0.5	308	0.1117	2	479.5682	488.6772	490.1917	484.6984	465.0851
129	0.5	3	24.97	0.5	308	0.1265	2	473.4552	482.2921	483.7614	478.4052	459.3426
130	0.5	3	24.05	0.5	308	0.1409	2	467.4213	475.9846	477.4075	472.1914	453.6851
131	0.5	3	23.15	0.5	308	0.1547	2	461.5372	469.83	471.2066	466.1314	448.1788
132	0.5	3	24.76	0.5	308	0	2.2	481.1984	489.8272	491.1491	485.4323	465.6951
133	0.5	3	26.36	0.5	308	0.007165	2.2	490.0122	499.0136	500.4081	494.5129	473.9745
134	0.5	3	27.45	0.5	308	0.01479	2.2	495.6983	504.9372	506.3786	500.3735	479.3223
135	0.5	3	28.16	0.5	308	0.02273	2.2	499.1357	508.5182	509.9879	503.9187	482.5558
136	0.5	3	28.56	0.5	308	0.03088	2.2	500.789	510.2413	511.7248	505.6265	484.1076
137	0.5	3	28.74	0.5	308	0.03914	2.2	501.2015	510.6728	512.1599	506.0561	484.4885
138	0.5	3	28.73	0.5	308	0.04746	2.2	500.5572	510.0043	511.4864	505.3973	483.8719
139	0.5	3	28.59	0.5	308	0.05577	2.2	499.2019	508.5955	510.0667	504.006	482.5851
140	0.5	3	28.35	0.5	308	0.06405	2.2	497.3027	506.6199	508.0758	502.0544	480.7865
141	0.5	3	27.66	0.5	308	0.08037	2.2	492.3742	501.4895	502.905	496.9866	476.1299
142	0.5	3	26.82	0.5	308	0.09627	2.2	486.6617	495.5392	496.9082	491.1124	470.7468
143	0.5	3	25.9	0.5	308	0.1117	2.2	480.5426	489.1614	490.4804	484.8202	464.9949
144	0.5	3	24.97	0.5	308	0.1265	2.2	474.4104	482.7662	484.035	478.5286	459.2444
145	0.5	3	24.05	0.5	308	0.1409	2.2	468.3602	476.4526	477.6721	472.3207	453.5842
146	0.5	3	23.15	0.5	308	0.1547	2.2	462.4565	470.2885	471.4598	466.2628	448.0738
147	0.5	3	24.76	0.5	308	0	2.5	485.7888	493.3928	487.5218	481.8975	462.3753
148	0.5	3	26.36	0.5	308	0.007165	2.5	487.5527	495.8787	499.6799	499.0057	478.0085
149	0.5	3	27.45	0.5	308	0.01479	2.5	496.861	505.111	505.3115	499.4318	478.254
150	0.5	3	28.16	0.5	308	0.02273	2.5	499.1125	507.7073	509.7463	504.2404	482.5915
151	0.5	3	28.56	0.5	308	0.03088	2.5	502.0073	510.5059	511.87	505.9387	484.1445
152	0.5	3	28.74	0.5	308	0.03914	2.5	502.4185	510.9412	512.3083	506.3743	484.532
153	0.5	3	28.73	0.5	308	0.04746	2.5	501.7936	510.3062	511.6709	505.7507	483.9482
154	0.5	3	28.59	0.5	308	0.05577	2.5	500.4357	508.9064	510.2617	504.3682	482.6723
155	0.5	3	28.35	0.5	308	0.06405	2.5	498.5278	506.9329	508.272	502.4179	480.8796
156	0.5	3	27.66	0.5	308	0.08037	2.5	493.5808	501.8096	503.1096	497.3543	476.2369
157	0.5	3	26.82	0.5	308	0.09627	2.5	487.8493	495.8674	497.1218	491.4845	470.8691
158	0.5	3	25.9	0.5	308	0.1117	2.5	481.7105	489.4972	490.702	485.1963	465.1325

Table A1. *Cont.*

Number	Gas Velocity (m/s)	Loading Capacity (kg)	Heating Power (W/kg)	Water Content (%)	Temper-ature (K)	He Content (mol/kg)	Metal Bulk Density (g/mL)	Container 1	Container 2	Container 3	Container 4	Container 5
159	0.5	3	24.97	0.5	308	0.1265	2.5	475.5602	483.1122	484.2693	478.898	459.3983
160	0.5	3	24.05	0.5	308	0.1409	2.5	469.4703	476.78	477.8861	472.6552	453.7289
161	0.5	3	23.15	0.5	308	0.1547	2.5	463.5415	470.6161	471.6764	466.5838	448.2252
162	0.5	3	29.47	0.5	308	0	2.2	511.0976	522.2425	516.2214	510.6872	488.9699
163	0.5	3	30.93	0.5	308	0.00852	2.2	515.6384	525.6774	527.2807	520.9109	498.1864
164	0.5	3	31.88	0.5	308	0.01746	2.2	520.1127	530.3315	531.9723	525.5268	502.4201
165	0.5	3	32.43	0.5	308	0.02667	2.2	522.3633	532.6723	534.3307	527.8506	504.5453
166	0.5	3	32.69	0.5	308	0.03604	2.2	523.0397	533.378	535.0417	528.5522	505.1754
167	0.5	3	32.72	0.5	308	0.04549	2.2	522.49	532.8096	534.4693	527.991	504.6419
168	0.5	3	32.57	0.5	308	0.05494	2.2	520.9929	531.2563	532.9039	526.453	503.209
169	0.5	3	32.29	0.5	308	0.06436	2.2	518.8185	528.9985	530.6285	524.2171	501.1349
170	0.5	3	31.92	0.5	308	0.07369	2.2	516.1824	526.2601	527.8687	521.5054	498.6253
171	0.5	3	30.98	0.5	308	0.09202	2.2	509.8882	519.7172	521.2748	515.0293	492.6474
172	0.5	3	29.89	0.5	308	0.1098	2.2	502.843	512.3884	513.8887	507.7804	485.9754
173	0.5	3	28.76	0.5	308	0.1269	2.2	495.6291	504.8786	506.3199	500.3582	479.1618
174	0.5	3	27.61	0.5	308	0.1434	2.2	488.3378	497.283	498.6646	492.8632	472.2941
175	0.5	3	26.5	0.5	308	0.1592	2.2	481.2999	489.9462	491.2704	485.6385	465.6823
176	0.5	3	25.43	0.5	308	0.1744	2.2	474.5082	482.8616	484.1302	478.6662	459.3176
177	0.5	2.6	28.74	0.5	298	0.03914	1.330565	488.0676	502.0149	505.4797	501.1105	485.3027
178	0.5	2.6	28.74	0.5	303	0.03914	1.330565	490.8527	504.6989	508.1357	503.8071	488.1229
179	0.5	2.6	28.74	0.5	308	0.03914	1.330565	493.6486	507.3937	510.8026	506.5143	490.9532
180	0.5	2.6	28.74	0.5	313	0.03914	1.330565	500.0682	514.1248	512.8479	513.0407	495.2577
181	0.5	2.6	28.74	0.5	318	0.03914	1.330565	503.0446	515.4956	515.112	514.2698	498.8061
182	0.5	2.6	28.74	0.5	323	0.03914	1.330565	505.8909	518.2272	517.8158	517.013	501.6729
183	0.5	2.8	32.72	1	298	0.04549	1.330565	513.4841	529.2146	533.0436	528.2633	510.436
184	0.5	2.8	32.72	1	303	0.04549	1.330565	516.2592	531.871	535.6601	530.924	513.2344
185	0.5	2.8	32.72	1	308	0.04549	1.330565	519.0386	534.5332	538.3175	533.6084	516.0389
186	0.5	2.8	32.72	1	313	0.04549	1.330565	521.8284	537.2078	540.9536	536.2868	518.8487
187	0.5	2.8	32.72	1	318	0.04549	1.330565	524.6245	539.888	543.5997	538.9739	521.6668
188	0.5	2.8	32.72	1	323	0.04549	1.330565	527.4299	542.5779	546.2572	541.6707	524.4939

References

1. Sims, H.E.; Webb, K.J.; Brown, J.; Morris, D.; Taylor, R.J. Hydrogen yields from water on the surface of plutonium dioxide. *J. Nucl. Mater.* **2013**, *437*, 359–364. [CrossRef]
2. Veirs, D.K. Gas generation from water adsorbed onto pure plutonium dioxide powder. *Mater. Res. Soc. Symp. Proc.* **2006**, *893*, 8930703. [CrossRef]
3. Haschke, J.M.; Allen, T.H.; Morales, L.A. Reaction of plutonium dioxide with water: Formation and properties of PuO_{2+x}. *Science* **2000**, *287*, 285–287. [CrossRef] [PubMed]
4. Bushuev, A.V. Determination of the plutonium mass in containers with plutonium dioxide according to the γ radiation from spontaneous-fission products. *At. Energy* **2010**, *108*, 46–52. [CrossRef]
5. Hirooka, S. Toward long-term storage of nuclear materials in MOX fuels fabrication facility. *Front. Nucl. Eng.* **2023**, *2*, 1119567. [CrossRef]
6. Rahman, H.S.; Hunter, T.N.; Heggs, P.J. Simplified heat transfer model for highly active raffinate contained in buffer storage tanks. *Chem. Eng. Res. Des.* **2023**, *190*, 464–475. [CrossRef]
7. Bae, J.; Bean, R.; Abboud, R. CFD analysis of a dry storage cask with advanced spent nuclear fuel cask additives. *Ann. Nucl. Energy* **2020**, *145*, 107610. [CrossRef]
8. Benavides, J.; Jimenez, G.; Galban, M.; Lioret, M. Methodology for thermal analysis of spent nuclear fuel dry cask using CFD codes. *Ann. Nucl. Energy* **2019**, *133*, 257–274. [CrossRef]
9. Zuo, Q.; Zhu, L.; Liu, J. Research and verification on CFD natural convection model of QM400. *Ann. Nucl. Energy* **2019**, *126*, 443–451. [CrossRef]
10. Tseng, Y.S.; Wang, J.R.; Tsai, F.P.; Cheng, Y.H.; Shih, C. Thermal design investigation of a new tube-type dry-storage system through CFD simulations. *Ann. Nucl. Energy* **2011**, *38*, 1088–1097. [CrossRef]
11. Maxwell, C.I.; Pencer, J. Molecular dynamics modelling of the thermal conductivity of off-stoichiometric $UO_{2\pm x}$ and $(U_yPu_{1-y})O_{2\pm x}$ using equilibrium molecular dynamics. *J. Ann. Nucl. Energy* **2019**, *131*, 317–324. [CrossRef]
12. *DOE-STD-3013-2012*; Stabilization, Packaging, and Storage of Plutonium-Bearing Materials. U.S. Department of Energy: Washington, DC, USA, 2012.
13. Wang, Y.H.; Lin, Y.P.; Chang, H.Y.; Lai, C.M. Ventilation pattern and heat dissipation characteristics of a vertical dry storage cask for spent nuclear fuel: Wind tunnel experiments and CFD simulations. *Ann. Nucl. Energy* **2021**, *160*, 108364. [CrossRef]
14. Tang, J.; Chen, J.; Liu, P. First principles study of oxygen diffusion in plutonium dioxide, sesquioxide, and their interface under activated conditions. *J. Nucl. Mater.* **2023**, *578*, 154348. [CrossRef]
15. Bottau, V.; Tondut, L.; Allinei, P.G.; Perot, B.; Eleon, C.; Carasco, C.; Stefano, R.D.; Faussier, G. High-Resolution Gamma Spectrometry of a Plutonium Bearing Waste Drum with High-Energy Reaction-Induced Gamma Rays. *IEEE Trans. Nucl. Sci.* **2020**, *67*, 575–584. [CrossRef]

Disclaimer/Publisher's Note: The statements, opinions and data contained in all publications are solely those of the individual author(s) and contributor(s) and not of MDPI and/or the editor(s). MDPI and/or the editor(s) disclaim responsibility for any injury to people or property resulting from any ideas, methods, instructions or products referred to in the content.